Electrode-stress-induced nanoscale disorder in Si quantum electronic devices

J. Park, Y. Ahn, J. A. Tilka, K. C. Sampson, D. E. Savage, J. R. Prance, C. B. Simmons, M. G. Lagally, S. N. Coppersmith, M. A. Eriksson, M. V. Holt, and P. G. Evans

---

Articles you may be interested in

Combining experiment and optical simulation in coherent X-ray nanobeam characterization of Si/SiGe semiconductor heterostructures
Journal of Applied Physics **120**, 015304 (2016); 10.1063/1.4955043

Valley splitting of single-electron Si MOS quantum dots
Applied Physics Letters **109**, 253101 (2016); 10.1063/1.4972514

Formation of strain-induced quantum dots in gated semiconductor nanostructures
AIP Advances **5**, 087107 (2015); 10.1063/1.4928320

Circuit quantum electrodynamics architecture for gate-defined quantum dots in silicon
Applied Physics Letters **110**, 043502 (2017); 10.1063/1.4974536

Dispersive readout of a silicon quantum dot with an accumulation-mode gate sensor
Applied Physics Letters **110**, 212101 (2017); 10.1063/1.4984224

A reconfigurable gate architecture for Si/SiGe quantum dots
Applied Physics Letters **106**, 223507 (2015); 10.1063/1.4922249

Electrode-stress-induced nanoscale disorder in Si quantum electronic devices

J. Park,[1] Y. Ahn,[1] J. A. Tilka,[1] K. C. Sampson,[1] D. E. Savage,[1] J. R. Prance,[2] C. B. Simmons,[2] M. G. Lagally,[1,2] S. N. Coppersmith,[2] M. A. Eriksson,[1,2] M. V. Holt,[3] and P. G. Evans[1,a]

[1]*Department of Materials Science and Engineering, University of Wisconsin-Madison, Madison, Wisconsin 53706, USA*
[2]*Department of Physics, University of Wisconsin-Madison, Madison, Wisconsin 53706, USA*
[3]*Center for Nanoscale Materials, Argonne National Laboratory, Argonne, Illinois 60439, USA*

Disorder in the potential-energy landscape presents a major obstacle to the more rapid development of semiconductor quantum device technologies. We report a large-magnitude source of disorder, beyond commonly considered unintentional background doping or fixed charge in oxide layers: nanoscale strain fields induced by residual stresses in nanopatterned metal gates. Quantitative analysis of synchrotron coherent hard x-ray nanobeam diffraction patterns reveals gate-induced curvature and strains up to 0.03% in a buried Si quantum well within a Si/SiGe heterostructure. Electrode stress presents both challenges to the design of devices and opportunities associated with the lateral manipulation of electronic energy levels. © *2016 Author(s). All article content, except where otherwise noted, is licensed under a Creative Commons Attribution (CC BY) license (http://creativecommons.org/licenses/by/4.0/).* [http://dx.doi.org/10.1063/1.4954054]

A new generation of devices based on the quantum properties of charge and spin in solids has the potential to improve dramatically the functional capabilities of nanoscale electronics.[1,2] Silicon is a particularly promising host material for this class of devices because of the precision with which electronic states in Si can be manipulated using elastic strain and applied fields. A robust fabrication path towards exploiting the favorable quantum properties of Si is to confine electrons within electrostatically defined quantum dots (QDs) created in a two-dimensional electron gas in a strained-Si quantum well (QW) within a Si/SiGe heterostructure.[1,3–6] Electrons in Si QDs exhibit long electron spin coherence times due to weak spin-orbit coupling and potentially low nuclear coupling because Si can have zero nuclear spin in isotopically purified Si, ideal conditions for quantum computing applications.[7] Quantum electronic devices in Si and all other semiconductors, however, regularly require extensive optimization of the gate voltages that control the device, in order to compensate for a disordered potential-energy landscape that is usually assumed to derive from unintentional background doping or fixed charge in oxide layers.

Here we show that the mechanical stress extrinsically introduced by the metal electrodes creates significant potential-energy disorder in gate-defined quantum devices, presenting a challenge to the design of such devices and offering a key target for device design. Using synchrotron hard x-ray nanobeam diffraction and nanoscale mechanical modeling, we find that the strain-induced nonuniformity has a magnitude that is comparable to the charging energy of quantum dots, and that for donor-based quantum devices the strain is large enough to produce significant donor-to-donor variation in the contact hyperfine interaction.

A common feature of the coupling between structural and electronic phenomena in quantum devices is that the relevant structural length scales range from a few nanometers up to the submicron

---

[a]Electronic mail: pgevans@wisc.edu

4, 066102-1

sizes of the full device. At the smallest scale, features such as interface atomic steps, strain variations, and compositional fluctuations modify either the energies of relevant quantum states or the rates of transitions between states, as predicted for example in the Si/SiGe system.[8] Imposed stresses resulting from surface features or macroscopic curvature similarly perturb the local electron energetics but can also lead to new device-scale phenomena such as modifications to ballistic transport, anisotropy in two-dimensional transport, and modulations of the potential induced by periodic surface structures.[9–11] Mechanically these perturbations due to surface structures can result from interface stresses produced by a combination of atomic-scale and microstructural effects in the thin films that are used to create electrodes or other device components.[12,13] Interface stress is a key aspect of the design of the present generation of silicon electronics, where the distortion is employed to increase the electron mobility by shifting the relative energies of silicon conduction band valleys.[14] Its effect in quantum devices, however, is not clear.

Some degree of variation also results from the synthesis of the host heterostructure, for example via the random nucleation of dislocations in plastic relaxation during Si/SiGe heteroepitaxy. Hard x-ray nanoprobe studies of the far-from-electrode regions of the strained-Si QW in a relaxed Si/SiGe heterostructure grown epitaxially on Si (001) have found that structural distortion from the plastically relaxed SiGe layer is transferred into the strained-Si QW.[15] The elastic stress resulting from the growth of the strained-Si QW on SiGe creates a strain due to bending with a magnitude of approximately 10^{-6}, which shifts the energy of electronic states by amounts sufficient to affect the rates of transitions between states.[15] A lateral variation of the structure of QWs is also observed in Si/SiGe QWs produced using other fabrication methods and in other semiconductor materials. The transfer of released elastically relaxed Si/SiGe heterostructures as nanomembranes onto new substrates occurs without distortion due to crystalline mosaic or other effects of plastic relaxation,[16,17] but is instead accompanied by distortion resulting from the transfer process.[18]

The distribution and magnitude of stress within silicon quantum devices can intuitively be expected to depend strongly on the device geometry and on the distance between the electrodes and the quantum well layer. Here we show that metal gate electrodes impose a stress that is elastically transferred to the strained-Si QW of a Si/SiGe quantum device. The strain resulting from an isolated narrow linear electrode, a nearly ideal model geometry, is in excellent agreement with elastic predictions. The distribution of strain around the pattern of electrodes from which electrostatic gates are fabricated has a more complex variation but shares the same fundamental origin.

Structural insight into strained semiconductors has been obtained in studies using x-ray techniques including micro- and nanobeam diffraction,[12,19–22] and ptychography,[23,24] reciprocal-space map analysis combined with finite element studies,[25,26] as well as through transmission electron microscopy.[27] Emerging x-ray ptychography techniques have the potential to provide images of strain fields using phase retrieval techniques, but have not yet been demonstrated for the case of complex heterostructures including both plastic relaxation and large lattice tilts. Future development of ptychography would complement the present approach by providing maps of strain as a function of depth, including through the Si quantum well. The structural results presented here are derived from synchrotron hard x-ray nanodiffraction conducted using the hard x-ray nanoprobe operated by the Center for Nanoscale Materials at Sector 26 of the Advanced Photon Source of Argonne National Laboratory, which allows the distortion of devices to be probed without perturbations due to sample preparation. Incident x-ray beams with 10 keV photon energy were focused to a spot size of 50 nm full width at half-maximum using 160 μm-diameter Fresnel zone plate with an outermost zone width of 30 nm. A center stop (diameter 60 μm) and order sorting aperture were used to attenuate unfocused radiation and x-rays focused to other orders of the zone plate. The high degree of spatial coherence in the incident x-ray beam allowed structural measurements to be performed with very high precision in spite of the large angular divergence of 0.24° introduced by the zone-plate focusing optics. Analysis methods for deriving structural insight in this situation are described below. Diffraction patterns were acquired using a charge-coupled-device (CCD) detector consisting of a 1024×1024 array of 13 μm pixels located at a distance of 0.69 m from the sample.

The Si/SiGe heterostructure in which the quantum dot device was fabricated consisted of a $Si_{1-x}Ge_x$ layer with a thickness of several μm grown on a Si (001) substrate with the Ge concentration graded linearly to $x = 0.3$ during growth. The $Si_{1-x}Ge_x$ layer relaxed during deposition
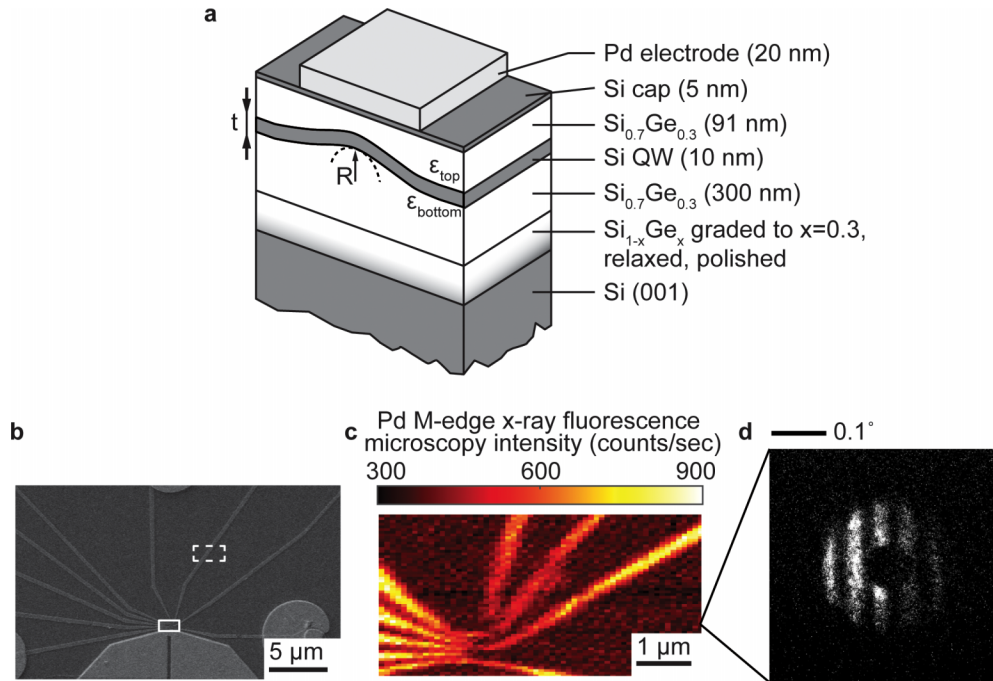
FIG. 1. (a) Cross section of the Si/SiGe heterostructure and Pd gate electrode, with layer thicknesses. A strain difference, ε_{bottom}-ε_{top}, arises across the thickness, t, of the strained-Si QW due to the electrode-induced radius of curvature R. (b) SEM image of the regions of interest. The x-ray nanodiffraction study was conducted in the areas indicated by the dashed and solid boxes. (c) X-ray nanobeam map of the Pd M-edge fluorescence intensity in the device region. (d) X-ray nanobeam diffraction pattern of the strained-Si QW acquired from the indicated area at a Bragg angle of 27.49°, approximately matching the Bragg reflection of the strained-Si QW.

through the formation of dislocations that appear as a characteristic cross-hatch structure.[16,17] Nanometer-scale height variations that do not lead to tilting of the lattice have been observed at the surfaces of SiGe layers due to the stress dependence of SiGe growth rate.[28] A subsequent Si/SiGe heterostructure (top 91 nm $Si_{0.7}Ge_{0.3}$, 10 nm strained-Si QW, 300 nm $Si_{0.7}Ge_{0.3}$ buffer) and a 5 nm Si cap layer were grown on the relaxed $Si_{1-x}Ge_x$ layers, as shown in Figure 1(a). Note that the thickness of the 91 nm $Si_{0.7}Ge_{0.3}$ layer is slightly different than the nominal design value of the thickness of that layer given in Ref. 15. The lattice mismatch between Si and the relaxed $Si_{0.7}Ge_{0.3}$ layer leads to a biaxial in-plane strain in the strained-Si QW with a magnitude of 1%. A pattern of thin-film Pd metal gate electrodes was defined using electron beam lithography and deposited using electron beam evaporation to form the electrostatically controlled QD structure.

The residual stress in the Pd electrodes was transferred to the Si/SiGe heterostructure producing a depth-dependent strain and curvature. The effect of the curvature can be quantified by considering the strain difference across the strained-Si QW layer, defined as the difference between strains at the bottom (ε_{bottom}) and top (ε_{top}) surfaces. This strain difference is given by t/R, where t is the thickness of the strained-Si QW and R is the radius of the curvature. A scanning electron microscopy (SEM) image and a map of the Pd M-edge fluorescence intensity acquired by scanning the focused x-ray beam across the device are shown in Figures 1(b) and 1(c), respectively. The two regions of interest for detailed study are indicated by the dashed and solid boxes in Figure 1(b), which correspond to regions in which the structural deformation is produced by (i) an isolated electrode thin film circuit connection and (ii) the complex overlapping stress fields of many gate electrodes.

A diffraction pattern acquired with the x-ray beam set at a Bragg angle of 27.49°, approximately the angular maximum of the diffracted intensity of the 004 x-ray reflection of the strained-Si QW, is shown in Figure 1(d). The distribution of diffracted intensity in the x-ray diffraction pattern exhibits a number of features linked to the large angular divergence of the focused incident x-rays,

which effectively leads to the sampling of a range of wavevectors for each angular setting of the incident x-ray beam.[18,29] A key result of the analysis of the diffraction experiment, as described in the supplementary material,[30] is that, under the conditions in which the diffraction pattern shown in Figure 1(d) was acquired, the intensity associated with the diffracted x-ray beam is shifted in angle by the tilt of the strained-Si QW lattice planes induced by elastic deformation. The relationship between the tilt and the angular displacement in the diffraction pattern depends on the direction of the angular displacement of the diffraction pattern on the x-ray detector.[21,31] The tilt of the lattice planes can be resolved into components that are perpendicular or parallel to the long axis of the electrode for further elastic analysis using the geometrical construction shown in the supplementary material.[27,30]

We first consider the distortion in the strained-Si QW induced by the isolated linear electrode. Figure 2(a) shows a map of the Pd M-edge fluorescence intensity within the region of the dashed box in Figure 1(b). Maxima in the fluorescence intensity are observed when the incident focused x-ray beam illuminates the Pd electrodes. Figure 2(b) shows a map of the perpendicular tilt component of the lattice planes in the same region as the fluorescence map. The tilt angle varies rapidly in the region of the electrode, reaching a maximum magnitude of $0.02°$ near the electrode. The reversal of the sign of the tilt that is apparent beneath the center of the electrode is characteristic of the distortion of the strained-Si QW by the elastically transferred electrode residual stress. From the sign of the displacement at each edge we determine that the bending is such that the strained-Si QW planes have concave-down curvature beneath the electrode. There is a small difference in the apparent position of the electrodes in the fluorescence and tilt images (Figures 2(a) and 2(b), respectively) due to the depth of strained-Si QW, as shown in the supplementary material.[27,30] A vector map, Figure 2(c), shows that the directions of the tilt are almost perpendicular to the length of the electrode. Regions far from the electrode exhibit a pattern of tilted mosaic blocks associated with the relaxation of the SiGe, as observed in previous nanobeam diffraction studies.[15]

The stress imparted on the strained-Si QW by the Pd electrode can be inferred from an elastic analysis of the distortion. Figure 2(d) shows the average tilt in the direction perpendicular to the length of the electrode as a function of the distance from the electrode. The small tilt difference between the start and end points of Figure 2(d) arises due to differences in the plastic relaxation of the bottom SiGe layer. Figure 2(d) includes a fit to the tilt using the edge force model, an analytical elastic analysis in which the residual stress in the electrode is elastically transferred to the substrate at the electrode edges.[32] This elastic model considers the ideal situation in which there is no contribution to the tilts arising from the spatial variation in plastic relaxation. The elastic analysis in Figure 2(d) makes the approximation that the Si/SiGe heterostructure can be accurately mechanically modeled as a single SiGe layer of uniform composition, which is appropriate given the thinness of the strained-Si QW layer. The tilt angle shown in Figure 2(d) is calculated from the displacement of the lattice planes at a depth of 100 nm under the electrode. The magnitude of the stress-thickness product that provides the best fit to the experimental data is 80 GPa Å, which is similar to reported stresses in metal thin films.[13,33,34]

The curvature of the strained-Si QW was extracted numerically from the perpendicular tilt component, and used to measure the strain difference between the bottom and the top of the strained-Si QW, as shown in Figure 2(e). The strain difference is positive when the in-plane lattice constant at the bottom of the strained-Si QW layer is larger than at the top. At the center of the electrode, the strain difference reaches its largest magnitude, 4×10^{-5}, corresponding to a radius of curvature of 250 μm. The strain is a factor of 10 larger than the previously reported strain difference arising from the plastic relaxation of SiGe alone.[15] More generally, the value of the elastic model lies in allowing other important aspects of the elastic distortion of the heterostructure to be predicted. For example, the difference in the strain between the region beneath the electrode and the region far from the electrode is shown in Fig. 2(f), providing insight that is useful in modeling the electronic effects arising from surface patterns.[35]

The elastic distortion of the region in which the electrode pattern defines the quantum dot is more complex than that of the single electrode. A Pd fluorescence map in the region of the QD is shown in Figure 3(a), encompassing the region indicated by the solid box in Figure 1(b). The positions of electrodes are outlined in Figure 3(a). The magnitude of the tilt within the quantum-dot
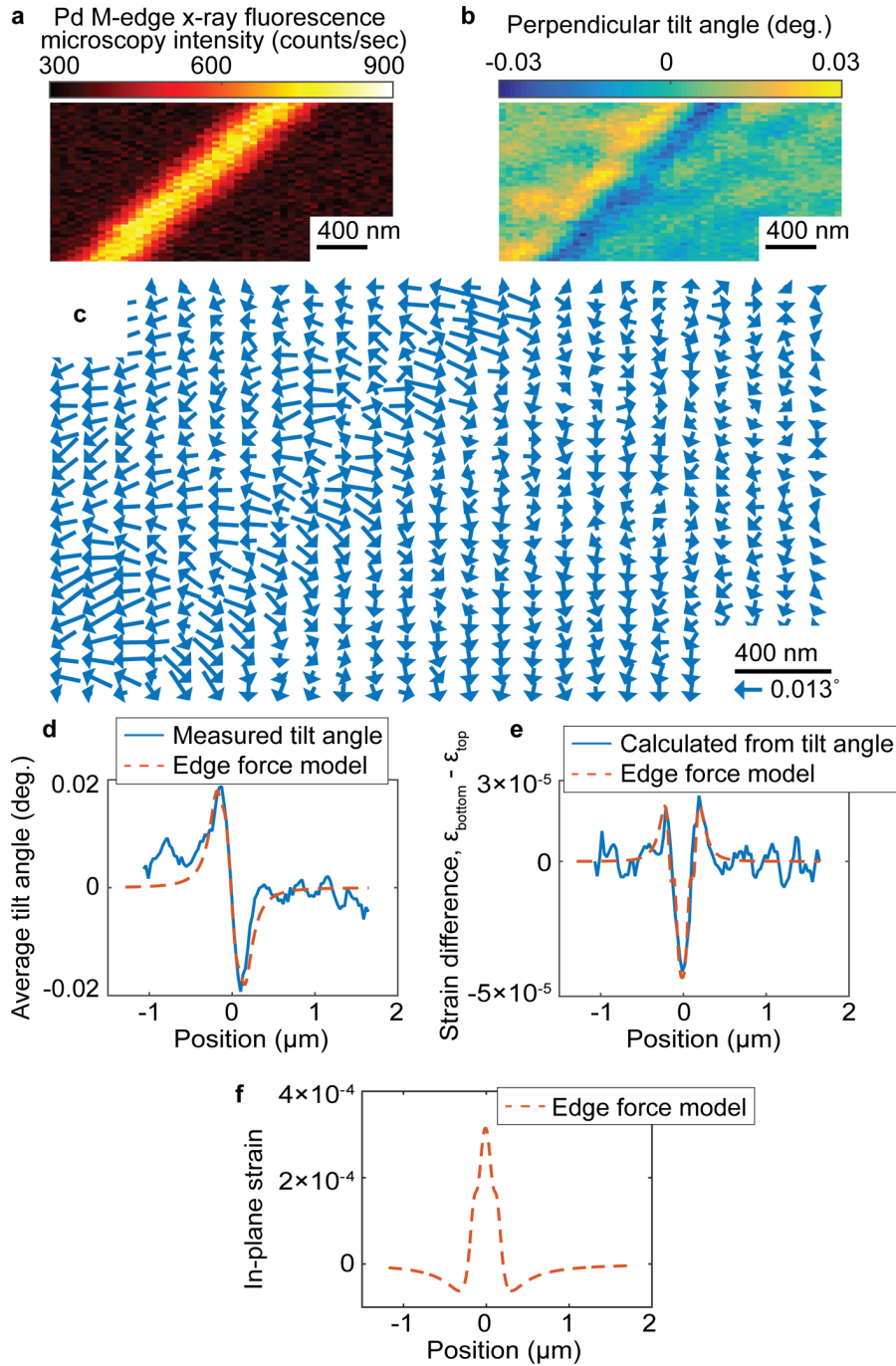
FIG. 2. (a) Map of the Pd M-edge fluorescence intensity in the region of a single linear Pd electrode. (b) Map of the perpendicular tilt component of the strained-Si QW lattice planes in the area shown in (a). (c) Map of the tilt orientation in the same area. The magnitude of the tilt can be interpreted using the key below the distance scale bar. (d) Comparison of measured average tilt angle and the edge force model of the elastic deformation. (e) Comparison between calculated strain difference of the strained-Si QW and the edge force model. (f) In-plane strain at the top strained-Si QW predicted by the elastic model.

region is shown in Figure 3(b). The tilt magnitude at the left side of the map where the five electrodes are closely spaced is 0.05°, a factor of 2.5 larger than at the edges of the single electrode. The structural deformation is larger in this area due to the overlap of the stress fields of adjacent electrodes, an effect previously observed at a much larger scale in metal test patterns on Si.[19]
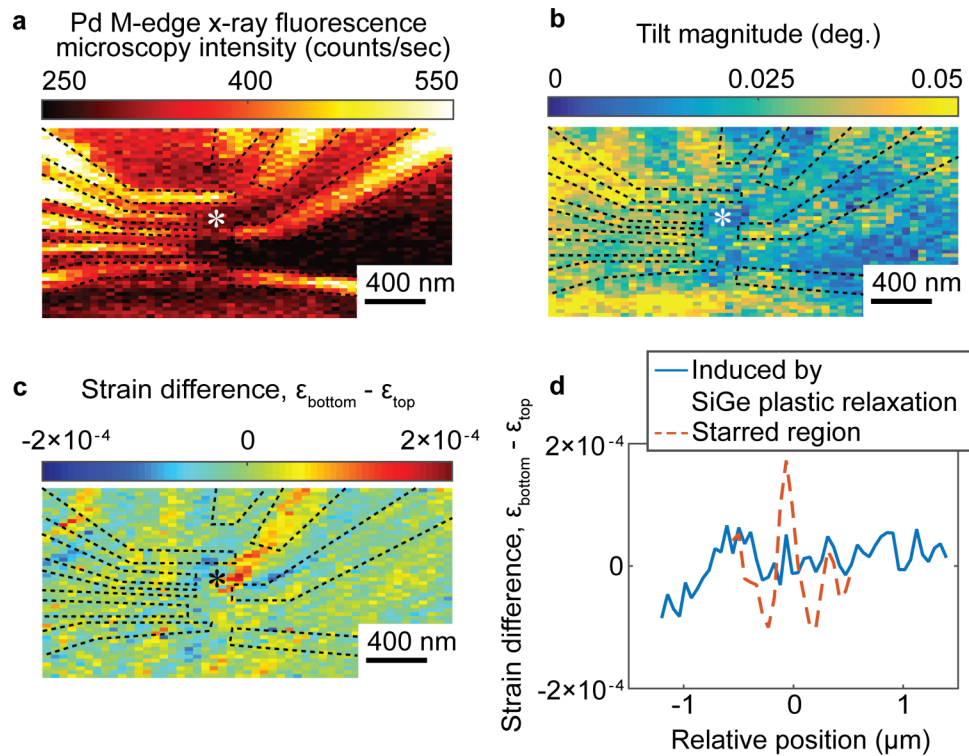
FIG. 3. (a) Map of the Pd M-edge fluorescence intensity in the region of the QD. (b) Tilt magnitude map of the strained-Si QW lattice planes in the area shown in (a). (c) Map of the strain difference across the thickness of the strained-Si QW. (d) Comparison between strain differences induced by the single electrode along with the intrinsic tilt from plastic relaxation of the SiGe layer (from Figure 2(b)) and the QD electrodes near the region indicated by the asterisk (from Figure 3(c)).

The strain difference in the region of the QD cannot be determined easily using an analytical mechanical model. The two-dimensional strain difference determined from the tilt angle information is in Figure 3(c). In this map, the strain difference reaches 10^{-4} at the point indicated with an asterisk, significantly larger than strain difference induced by the single electrode. The strain difference profile for the single electrodes and the QD areas is compared in Figure 3(d), using the strain differences computed using the tilt information along the bottom of the tilt image in Figure 2(b) and in the vicinity of the asterisk in Figure 3(c), respectively.

The deformation due to the electrodes also leads to a further distinctive feature in x-ray diffraction patterns, besides overall angular shift described above. This effect can best be illustrated by comparing the regions near the electrodes with those of the unprocessed Si QW heterostructure. In areas far from the tilted near-electrode region, superimposed fringes appear in the diffraction pattern arising from the interference of the thickness fringes of the top SiGe layer with the broad diffraction feature associated with the strained-Si QW, as in Figure 4(a). A simulated diffraction pattern illustrating the interference effect is shown in Figure 4(b), produced using a method described by Ying *et al.*[29] The spacing of the fringes corresponds to a reciprocal-space separation of $\Delta q_z = 0.007$ Å^{-1}, matching the separation due to the thickness of the top SiGe layer. Note that the thickness fringes arising from the strained-Si QW are widely separated in reciprocal-space (by $\Delta q_z = 0.063$ Å^{-1}), and do not appear in the $\Delta q_z = 0.038$ Å^{-1} span of Figures 4(a) and 4(b).

The intensity fringes arising from the SiGe layer is not apparent in tilted regions, as illustrated in Figure 4(c). The top and bottom interfaces of the SiGe layer are not parallel in regions of electrode-induced tilt and the interference required to produce the fringes does not occur. The visibility of the thickness fringes in the diffraction pattern can be quantified by evaluating the Fourier component of the image at the spatial frequency corresponding to the thickness fringe spacing, using methods described in the supplementary material.[30] In Figures 4(d), a map of fringe visibility
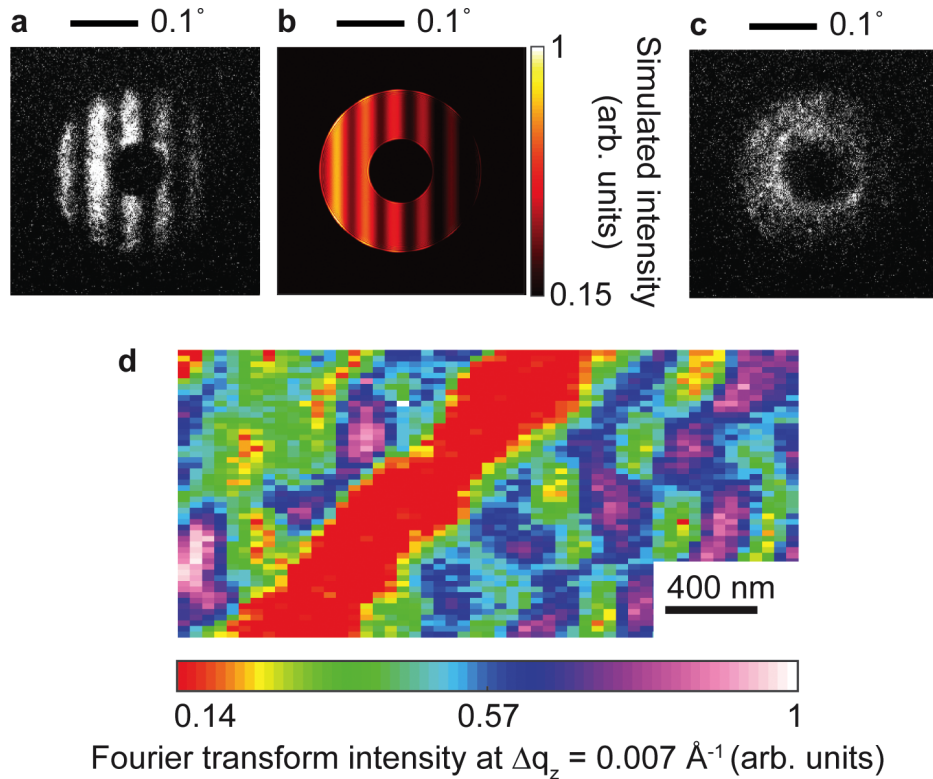
FIG. 4. (a) Diffraction patterns of the strained-Si QW in a location far from the tilted region. (b) Simulated diffraction pattern using the method of Ref. 29. (c) Diffraction pattern acquired at the tilted region. Both diffraction patterns were acquired at scattering wavevector $q_z = 4.65$ Å^{-1}, corresponding to a Bragg angle of 27.49°. (d) Fourier transform intensity at fringe spacing, $\Delta q_z = 0.007$ Å^{-1} exhibiting the disappearance of the SiGe-layer interference fringes in the tilted regions.

shows that the fringes in the diffraction pattern are reduced in intensity not only in the tilted region under the Pd single electrode but also at boundaries of cross-hatch regions far from the electrode. Thus, the fringe visibility map is a second readily apparent indicator of the structural deformation of the Si QW.

The results presented here show that significant structural deformation of strained-Si QW in Si/SiGe heterostructures arises not only from the plastic relaxation of the SiGe substrate layers but also from the stresses elastically transferred from the deposited electrodes. The transferred stresses lead to a strain difference of 10^{-4} over the thickness of the layer, which is a factor of 100 larger than the strain difference arising from the plastic relaxation of the SiGe substrate. The lateral variation of the strain is of a similar magnitude. From the perspective of an electron occupying the gate electrode-defined quantum dot, this variation in strain contributes a spatially varying potential-energy landscape with a peak-to-peak amplitude of 1.4 meV, of the same order of magnitude as the charging energy in few-electron quantum dots.[36] Thus, gate electrode-induced strain variation is a significant source of disorder in gate electrode-defined semiconductor quantum electronics.

In addition to its direct effect on the energy landscape in quantum devices, strain modifies the hyperfine interaction for electrons bound to donors,[37] of which phosphorous has received the most attention as a prototype qubit.[38] Depending on the initial strain condition of the host Si lattice, strain variations of 10^{-4} can lead to fractional variations in the hyperfine coupling as large as 2.5%, leading to variations in the electron spin resonance frequency of order 2 MHz, far larger than the 2 kHz linewidth of an individual donor in isotopically purified ^{28}Si,[39] with significant implications for addressing multiple nearby donor-bound electron spin qubits.

The deposition of thin-film electrodes is an inevitable part for QD fabrication and thus there will be a structural deformation of the QW in a wide range of quantum electronic devices fabricated

from Si and other semiconductors, including, in addition to qubits, spin charge-coupled devices (CCDs) and structures exhibiting quantum effects in transport.[10,40] The strain variation has the potential to introduce spatial nonuniformity of the energies of strained-Si QW states and could have a negative impact on devices that do not account for mechanical deformation. In other systems, however, including GaAs heterostructures, lateral strain variation can be integrated into the design of materials and devices through lithographic patterns or through self-assembly.[41,25,26] With precise structural measurements, Si/SiGe materials and gate electrode patterns can in principle be designed to control the electrode-induced strain from the electrodes, and can provide an additional way to control the electronic properties of Si quantum materials.

[1] F. A. Zwanenburg, A. S. Dzurak, A. Morello, M. Y. Simmons, L. C. L. Hollenberg, G. Klimeck, S. Rogge, S. N. Coppersmith, and M. A. Eriksson, Rev. Mod. Phys. **85**, 961 (2013).

[2] L. R. Schreiber and H. Bluhm, Nat. Nanotechnol. **9**, 966 (2014).

[3] B. M. Maune, M. G. Borselli, B. Huang, T. D. Ladd, P. W. Deelman, K. S. Holabird, A. A. Kiselev, I. Alvarado-Rodriguez, R. S. Ross, A. E. Schmitz, M. Sokolich, C. A. Watson, M. F. Gyure, and A. T. Hunter, Nature **481**, 344 (2012).

[4] E. Kawakami, P. Scarlino, D. R. Ward, F. R. Braakman, D. E. Savage, M. G. Lagally, M. Friesen, S. N. Coppersmith, M. A. Eriksson, and L. M. K. Vandersypen, Nat. Nanotechnol. **9**, 666 (2014).

[5] D. Kim, Z. Shi, C. B. Simmons, D. R. Ward, J. R. Prance, T. S. Koh, J. K. Gamble, D. E. Savage, M. G. Lagally, M. Friesen, S. N. Coppersmith, and M. A. Eriksson, Nature **511**, 70 (2014).

[6] K. Eng, T. D. Ladd, A. Smith, M. G. Borselli, A. A. Kiselev, B. H. Fong, K. S. Holabird, T. M. Hazard, B. Huang, P. W. Deelman, I. Milosavljevic, A. E. Schmitz, R. S. Ross, M. F. Gyure, and A. T. Hunter, Sci. Adv. **1**, e1400254 (2015).

[7] J. J. Morton, D. R. McCamey, M. A. Eriksson, and S. A. Lyon, Nature **479**, 345 (2011).

[8] M. Friesen, M. A. Eriksson, and S. N. Coppersmith, Appl. Phys. Lett. **89**, 202106 (2006).

[9] D. Kamburov, H. Shapourian, M. Shayegan, L. N. Pfeiffer, K. W. West, K. W. Baldwin, and R. Winkler, Phys. Rev. B **85**, 121305 (2012).

[10] R. L. Willett, J. W. P. Hsu, D. Natelson, K. W. West, and L. N. Pfeiffer, Phys. Rev. Lett. **87**, 126803 (2001).

[11] B. Novakovic, R. Akis, and I. Knezevic, Phys. Rev. B **84**, 195419 (2011).

[12] K. Haruta and W. J. Spencer, J. Appl. Phys. **37**, 2232 (1966).

[13] G. Guisbiers, O. V. Overschelde, M. Wautelet, P. Leclère, and R. Lazzaroni, J. Phys. D: Appl. Phys. **40**, 1077 (2007).

[14] M. V. Fischetti, Z. Ren, P. M. Solomon, M. Yang, and K. Rim, J. Appl. Phys. **94**, 1079 (2003).

[15] P. G. Evans, D. E. Savage, J. R. Prance, C. B. Simmons, M. G. Lagally, S. N. Coppersmith, M. A. Eriksson, and T. U. Schulli, Adv. Mater. **24**, 5217 (2012).

[16] M. A. Lutz, R. M. Feenstra, F. K. LeGoues, P. M. Mooney, and J. O. Chu, Appl. Phys. Lett. **66**, 724 (1995).

[17] P. M. Mooney, J. L. Jordan-Sweet, and S. H. Christiansen, Appl. Phys. Lett. **79**, 2363 (2001).

[18] D. M. Paskiewicz, D. E. Savage, M. V. Holt, P. G. Evans, and M. G. Lagally, Sci. Rep. **4**, 4218 (2014).

[19] I. C. Noyan, P. C. Wang, S. K. Kaldor, and J. L. Jordan-Sweet, Appl. Phys. Lett. **74**, 2352 (1999).

[20] C. E. Murray, I. C. Noyan, P. M. Mooney, B. Lai, and Z. Cai, Appl. Phys. Lett. **83**, 4163 (2003).

[21] P. G. Evans, P. P. Rugheimer, M. G. Lagally, C. H. Lee, A. Lal, Y. Xiao, B. Lai, and Z. Cai, J. Appl. Phys. **97**(10), 103501 (2005).

[22] C. E. Murray, A. Ying, S. M. Polvino, I. C. Noyan, M. Holt, and J. Maser, J. Appl. Phys. **109**, 083543 (2011).

[23] M. V. Holt, S. O. Hruszkewycz, C. E. Murray, J. R. Holt, D. M. Paskiewicz, and P. H. Fuoss, Phys. Rev. Lett. **112**, 165502 (2014).

[24] S. O. Hruszkewycz, M. V. Holt, C. E. Murray, J. Bruley, J. Holt, A. Tripathi, O. G. Shpyrko, I. McNulty, M. J. Highland, and P. H. Fuoss, Nano Lett. **12**, 5148 (2012).

[25] N. Hrauda, J. Zhang, E. Wintersberger, T. Etzelstorfer, B. Mandl, J. Stangl, D. Carbone, V. Holy, V. Jovanovic, C. Biasotto, L. K. Nanver, J. Moers, D. Grutzmacher, and G. Bauer, Nano Lett. **11**, 2875 (2011).

[26] L. K. Nanver, V. Jovanović, C. Biasotto, J. Moers, D. Grützmacher, J. J. Zhang, N. Hrauda, M. Stoffel, F. Pezzoli, O. G. Schmidt, L. Miglio, H. Kosina, A. Marzegalli, G. Vastola, G. Mussler, J. Stangl, G. Bauer, J. van der Cingel, and E. Bonera, Solid State Electron. **60**, 75 (2011).

[27] M. Hytch, F. Houdellier, F. Hue, and E. Snoeck, Nature **453**, 1086 (2008).

[28] K. Sawano, S. Koh, Y. Shiraki, N. Usami, and K. Nakagawa, Appl. Phys. Lett. **83**, 4339 (2003).

[29] A. Ying, B. Osting, I. C. Noyan, C. E. Murray, M. Holt, and J. Maser, J. Appl. Cryst. **43**, 587 (2010).

[30] See supplementary material at http://dx.doi.org/10.1063/1.4954054 for description of imaging artifacts, and detailed analysis of the angular tilt and Fourier transform of diffraction patterns.

[31] G. A. Chahine, M.-I. Richard, R. A. Homs-Regojo, T. N. Tran-Caliste, D. Carbone, V. L. R. Jacques, R. Grifone, P. Boesecke, J. Katzer, I. Costina, H. Djazouli, T. Schroeder, and T. U. Schülli, J. Appl. Cryst. **47**, 762 (2014).

[32] I. A. Blech, J. Appl. Phys. **38**, 2913 (1967).

[33] J. A. Floro, S. J. Hearne, J. A. Hunter, P. Kotula, E. Chason, S. C. Seel, and C. V. Thompson, J. Appl. Phys. **89**, 4886 (2001).

[34] E. Chason, B. W. Sheldon, L. B. Freund, J. A. Floro, and S. J. Hearne, Phys. Rev. Lett. **88**, 156103 (2002).

[35] T. Thorbeck and N. M. Zimmerman, AIP Adv. **5**, 087107 (2015).

[36] F. Schaffler, Semicond. Sci. Technol. **12**, 1515 (1997).

[37] H. Huebl, A. R. Stegner, M. Stutzmann, M. S. Brandt, G. Vogg, F. Bensch, E. Rauls, and U. Gerstmann, Phys. Rev. Lett. **97**, 166402 (2006).

[38] J. J. Pla, K. Y. Tan, J. P. Dehollain, W. H. Lim, J. J. Morton, D. N. Jamieson, A. S. Dzurak, and A. Morello, Nature **489**, 541 (2012).

[39] J. T. Muhonen, J. P. Dehollain, A. Laucht, F. E. Hudson, R. Kalra, T. Sekiguchi, K. M. Itoh, D. N. Jamieson, J. C. McCallum, A. S. Dzurak, and A. Morello, Nat. Nanotechnol. **9**, 986 (2014).

[40] T. A. Baart, M. Shafiei, T. Fujita, C. Reichl, W. Wegscheider, and L. M. K. Vandersypen, Nat. Nanotechnol. **11**, 330 (2016).

[41] J. H. Davies and I. A. Larkin, Phys. Rev. B **49**, 4800 (1994).